Study of irregular roughness in minimal channels

J. Yang[1], *A. Stroh*[1], *S. Jakirlić*[2], *B. Frohnapfel*[1] *and P. Forooghi*[3,*]

[1]*Institute of Fluid Mechanics, Karlsruhe Institute of Technology, Germany*
[2]*Institute of Fluid Mechanics & Aerodynamics, Technical University Darmstadt, Germany*
[3]*Dept. of Mechanical & Production Engineering, Aarhus University, Denmark*

Abstract

Direct numerical simulation (DNS) is carried out to study turbulent flow over irregular rough surfaces in periodic minimal channels. A passive scalar transport equation is solved to study heat transfer over rough surfaces with the Prandtl number $Pr = 0.7$. The generation of irregular roughness is based on a mathematical randomization algorithm, in which the power spectrum (PS) of the roughness height function along with its probability density function (PDF) can be directly prescribed. The hydrodynamic and thermal properties of the roughness, particularly the roughness function (ΔU^+) as well as the temperature profile offset ($\Delta\Theta^+$), are compared with those obtained from a full span DNS for 6 types of roughness topographies with systematically varied PDF and PS configurations at $Re_\tau \approx 500$. The comparison confirms the ability of the minimal channel approach to perform characterization of irregular rough surfaces providing excellent agreement (within 5%) in ΔU^+ and $\Delta\Theta^+$ across various types of roughness topographies. Results also indicate that random realizations of roughness, with a fixed PS and PDF, translate to similar prediction with a narrow scatter. Finally, the impact of systematically varied roughness PDF and PS to both velocity and temperature profile is shown. It is also demonstrated that the influence of varying PDF and PS on the velocity and temperature fields is different.

1 Introduction

Rough surfaces are abundant in nature and engineering applications. It is well established that the topography of roughness can significantly affect its hydrodynamic properties. In practice, the most important hydrodynamic effect of roughness is an increase in the skin friction coefficient of the surface. This increase manifests itself in a downward shift in the logarithmic region of inner scaled mean velocity profile ΔU^+. The shifted velocity profile in logarithmic layer writes:

$$U^+ = \frac{1}{\kappa}\log(y^+) + A_m - \Delta U^+ \,. \qquad (1)$$

*Corresponding author's Email: forooghi@mpe.au.dk

Where $\kappa \approx 0.4$ is the von Karman constant, A_m is the smooth-wall offset. ΔU^+ is related to the equivalent sand-grain roughness k_s (Jiménez 2004); the latter parameter is widely used as an input to engineering applications. Furthermore, $\Delta U^+ = \sqrt{2/C_{fs}} - \sqrt{2/C_{fr}}$ gives direct relation between roughness function and skin friction (Hama 1954), where C_{fs}, C_{fr} are the skin friction coefficients for smooth and rough wall at matched Re_τ respectively. Therefore, the central importance of this mean velocity downward shift ΔU^+, which is referred to as the (Hama) roughness function in determining the hydrodynamic property of the roughness is understood. To find ΔU^+ for an arbitrary roughness at a certain roughness flow regime, one needs to either run a laboratory (or high-fidelity numerical) experiment or use a so-called roughness correlation, which relates the topography of roughness to ΔU^+. While the latter option is obviously less costly, large number of topographical metrics should be systematically investigated to construct such a predictive correlation e.g. the skewness $Sk = (1/k_{\text{rms}}^3)\int_S (k - k_{\text{md}})^3 \mathrm{d}S$ and $k_{\text{rms}} = \sqrt{(1/S)\int_S (k - k_{\text{md}})^2 \mathrm{d}S}$ (Flack & Schultz 2010), the effective slope ES$= (1/S)\int_S |\partial k/\partial x| \mathrm{d}S$ (Napoli *et al.* 2008) or the roughness correlation length L_{corr} (Sigal & Danberg 2008).

Similar to the skin friction, roughness can enhance the heat transfer in a fluidic system, and in fact designed roughness is often used in engineering application to enhance the heat transfer (Forooghi *et al.* 2017a). However, it is widely understood that the enhancement of heat transfer, reflected by Stanton number St, is not directly proportional to the increase of skin friction coefficient C_f due to the lack of the pressure-related term on the temperature side (Dipprey & Sabersky 1963). This can be reflected by applying the Reynolds analogy factor $RA = 2St/C_f$ (Bons 2005). The enhancement of heat transfer would result in a downward shift of the logarithmic temperature profile. Analogous to the Eqn. 1 the shifted rough wall temperature profile writes:

$$\frac{\Theta - \Theta_w}{\Theta_\tau} = \frac{1}{\kappa_h}\log(y^+) + A_h(Pr) - \Delta\Theta^+ \,, \qquad (2)$$

where Θ represents the non-dimensional temperature, the offset A_h depends on the molecular Pandtl number Pr, Θ_w is the temperature at wall, Θ_τ is the friction temperature $\Theta_\tau \equiv (q_w/\rho c_p)/U_\tau$. q_w is the temporally and spatially averaged wall heat flux and c_p is the specific heat capacity at constant pressure. Thus, the augmentation of heat transfer of a rough wall can be characterized by an analogous term to the roughness function ΔU^+, i.e. $\Delta\Theta^+$. The Stanton number for a rough surface, St_r, can be derived by $\Delta\Theta^+$ with known C_{fr} at a matched Re_τ through (MacDonald *et al.* 2019):

$$\Delta\Theta^+ = \sqrt{\frac{C_{fs}}{2}}\left(\frac{1}{St_s} - \frac{1}{\kappa\kappa_h}\right) - \sqrt{\frac{C_{fr}}{2}}\left(\frac{1}{St_r} - \frac{1}{\kappa\kappa_h}\right). \tag{3}$$

where C_{fs} and St_s are the skin friction coefficient and Stanton number for the smooth wall, respectively.

It has long been desired for an *a priori* prediction of the aforementioned quantities to avoid resource demanding (numerical) experiments. Flack proposed use of Direct Numerical Simulation (DNS) for generating massive database needed for a universal roughness correlation (Flack 2018). The major problems in reaching this goal are the high computational cost of the DNS approach and difficulties related to the measurement of realistic rough surfaces. Such roughness scans are rare and mostly unsuitable for systematic studies. The aim of this work is to examine a new framework, which overcomes both obstacles. To relieve the computational cost we simulate the flow in fully developed turbulent channels with reduced streamwise and spanwise sizes. The idea was previously established and validated by Chung *et al.* (2015), MacDonald *et al.* (2016, 2019) with sinusoidal roughness structure. The criteria of the minimal channel size is given by those authors: $L_z^+ \geq \max(100, \tilde{k}^+/0.4, \lambda_{\text{sin}}^+)$, $L_x^+ \geq \max(1000, 3L_z^+, \lambda_{\text{sin}}^+)$, where L_x and L_z are the streamwise and spanwise extend of the channel, respectively and $\tilde{k}$ is the amplitude of the sinusoidal structure. λ_{sin} represents the wavelength of the sinusoidal structure. The criteria are set with the aim of accommodating the minimal channel to the near wall turbulence as well as the roughness structure. The research shows that minimal channel following the criteria above is capable for this type of roughness (repetitive) structure to predict the roughness function ΔU^+ as well as the temperature offset $\Delta\Theta^+$, but has not been examined for irregular roughness up to now. Therefore, the effect of repeating irregular roughness and the limited sample size of irregular roughness topography introduced by the significantly reduced spanwise extend of minimal channel is yet unknown.

In order to evaluate the validity of this approach for irregular rough surfaces we employ the random algorithm proposed by Pérez-Ràfols & Almqvist (2019) for generation of roughness. With the roughness generation method surface is generated randomly while the roughness statistical properties can be controlled by its height probability density function (PDF) and the power spectrum (PS) (hence the term pseudo-random roughness). The generation process is realized by discrete fast Fourier transform (DFFT), thus it is inherently suitable for the DNS simulations where periodic boundary condition is required.

In the present work, pseudo-random roughness with variation of PDF and PS are generated and simulated in both minimal channels and conventional full-span channels at $Re_\tau \approx 500$. The performance of the roughness generation method as well as the minimal channels are demonstrated. The impact of different roughness height PDF and PS configurations on both velocity and temperature fields is analyzed.

2 Methodology

Pseudo-random roughness generation method

The pseudo-random roughness is generated with the method originally proposed by Pérez-Ràfols & Almqvist (2019). The roughness height function is represented by discrete elevation map on 2-D Cartesian grid, i.e. $k(x, z)$, where x, z are the streamwise and spanwise coordinate respectively. Initially, a roughness map with prescribed roughness PDF is given and is labeled as k^0_{PDF}. This map does not necessarily contain desired PS. For the next step, this map is transformed using DFFT and compared with the second initial map with desired PS, which is labeled as k^0_{PS}. After that, the field is transformed back with inverse DFFT and the height distribution is adjusted to fit the PDF. The iterative adjustment of PDF and PS continues until the error, which is measured by the devation in PDF and PS profile, approaches a stationary low value. For further information readers are referred to the manuscript by Pérez-Ràfols & Almqvist, 2019.

Direct numerical simulation

Direct numerical simulations are carried out in a fully developed turbulent channel. The flow is driven by constant pressure gradient P_x. Periodic boundary condition is applied in the streamwise and spanwise directions of the channel, while the upper and lower walls are covered by the roughness structures. The roughness with no-slip & zero-temperature boundary condition is realized by imposing immersed boundary method

(IBM) following Goldstein's method (Goldstein 1993), where additional force is applied to the flow within the roughness elements to obtain zero velocity & temperature inside the roughness. A source term Q is added to the energy equation for the simulation of mixed-type thermal boundary condition (the approach proposed by Kasagi *et al.*, 1992). Thus, the Navier-Stokes equation writes:

$$\nabla \cdot \mathbf{u} = 0 \,, \tag{4}$$

$$\frac{\partial \mathbf{u}}{\partial t} + \nabla \cdot (\mathbf{u}\mathbf{u}) = -\frac{1}{\rho}\nabla p + \nu \nabla^2 \mathbf{u} - \frac{1}{\rho} P_x \hat{\mathbf{e}}_x + \mathbf{F}_u \,, \tag{5}$$

$$\frac{\partial \theta}{\partial t} + \nabla \cdot (\mathbf{u}\theta) = \alpha \nabla^2 \theta + Q + \mathbf{F}_\theta \,, \tag{6}$$

where $\mathbf{u}$ is the velocity vector $\mathbf{u} = (u, v, w)^\intercal$. P_x is the mean pressure gradient in the flow direction added as a constant and uniform source term to the momentum equation to drive the flow in the channel. Here p, $\hat{\mathbf{e}}_x$, ρ, ν, $\mathbf{F}_\theta$ and $\mathbf{F}_u$ are pressure fluctuation, Kronecker delta, density, kinematic viscosity and external source term for momentum and energy equation due to IBM, respectively. The Friction Reynolds number is defined as $Re_\tau = u_\tau(H - k_{\mathrm{md}})/\nu$, where $u_\tau = \sqrt{\tau_w/\rho}$ is the friction velocity and $\tau_w = -P_x(H - k_{\mathrm{md}})$ is the wall shear stress prescribed by the constant pressure gradient.

Description of cases

Thanks to the flexibility of the roughness generation method, two of the roughness parameters chosen from both PDF and PS sides are systematically varied and analyzed utilizing DNS, namely Sk and the PS slope p. Three values of Sk are selected i.e. $Sk \approx -0.48$, 0, 0.48. Skewed roughness distribution obeys Weibull's distribution $f_W(k) = K\beta^K k^{(K-1)} e^{-(\beta k)^K}$, where K is the form factor which is adjusted to match desired Sk, non-skewed roughness obeys the Gaussian distribution $f_G(k) = e^{-(1/2)(k-\mu/\sigma)^2}/(1/\sigma\sqrt{2\pi})$. Moreover the kurtosis $Ku \approx 3$ is selected for all roughness in search of the similarity to the Gaussian distribution. Therefore, the PDF are characterized in terms of negatively skewed, Gaussian and positively skewed distribution. The height of the roughness is scaled by the the 99% confidence interval of the PDF, which is denoted as k_{99}. $k_{99} = 0.1H$ is prescribed to all roughness configurations. In order to avoid extreme high/low roughness, roughness elements locate out side $1.2 \times k_{99}/2$ around the meltdown height $k_{md} = (1/S)\int_S k \mathrm{d}S$ are excluded.

On the other side, power-law PS is employed, i.e. $E_k(\mathbf{q}) = C_0(\|\mathbf{q}\|/q_0)^p$, where $\mathbf{q}$ is the wavenumber vector $\mathbf{q} = (q_x, q_z)^\intercal$, $q_0 = 2\pi/\lambda_0$ is the reference wavenumber corresponding to the largest in-plane length scale λ_0, C_0 is a constant to scale the roughness height, and p is the slope of the power-law PS. p is chosen as -1 and -2 in seek of overlapping with previous researches (Barros *et al.* 2018, Nikora *et al.*, 2019). The cutoff wavelengths of the PS are selected to accommodate to the channel size as well as the grid resolution, i.e. the presenting roughness wavelength λ obeys $0.8H \leq \lambda \leq 0.08H$.

In summary, by systematically investigating of these two roughness parameters in different channel sizes, in total 12 (3 PDF $\times$ 2 PS $\times$ 2 sizes) rough surfaces are individually produced. Following abbreviation is used throughout the text to distinguish the cases:

$$\overbrace{\underbrace{G}_{\text{PDF}}\,\underbrace{2}_{-p}}^{\text{Topography}} \,|\, \overbrace{F}^{\text{Channel size}} \,. \tag{7}$$

- The first character indicates the type of PDF; G for Gaussian distribution, P for positively skewed ($Sk \approx 0.48$), and N for negatively skewed ($Sk \approx -0.48$).
- The second digit indicates the PS slope; 1 for $p = -1$ and 2 for $p = -2$.
- The following character(s) indicates the channel size; F for full channel ($8H \times 4H$), M for the minimal channel ($2.4H \times 0.8H$)

One of the irregular roughness topographies, $G2F$, is illustrated for full-sized DNS in figure 1, the size of the minimal channel is represented by the black frame in the figure. The roughness metrics that are widely used for roughness characterization are shown in Table 1. As one can see, the roughness topographical statistics from the random generation process are preserved for both surface sizes. It is worth mentioning that the roughness for minimal channels and full span channels are independently generated, which means each surface has an individual realization but the statistics are controlled by the generation method. Thus, the stability of the generation method is demonstrated in terms of roughness topographical statistics.

3 Results

The DNS results, specifically the mean velocity and temperature profiles, $U(y)$ and $\Theta(y)$ are obtained by applying averaging in wall-parallel directions and time.

Furthermore, due to the irregularity of surface structure the origin of the wall normal coordinate of a rough surface cannot be naturally defined. To this end, Jackson (1981) proposed use of moment centroid of the drag profile on rough surfaces as the virtual origin to align the logarithmic velocity

Topography	Sk	p	k_{md}/H	k_{rms}/H	L_x^{corr}/H	S_f/S	ES	ΔU^+	$\Delta\Theta^+$
$P1F$	0.48	-1	0.046	0.0208	0.052	0.28	0.57	7.33	4.17
$P1M$	0.48	-1	0.046	0.0208	0.056	0.28	0.55	7.28	4.19
$P2F$	0.48	-2	0.046	0.0208	0.100	0.21	0.44	6.99	3.82
$P2M$	0.48	-2	0.046	0.0208	0.110	0.20	0.40	6.86	3.84
$G1F$	0	-1	0.061	0.0200	0.050	0.27	0.54	6.67	3.93
$G1M$	0	-1	0.061	0.0200	0.054	0.27	0.53	6.66	3.99
$G2F$	0	-2	0.061	0.0200	0.100	0.20	0.43	6.30	3.62
$G2M$	0	-2	0.061	0.0200	0.108	0.19	0.40	6.39	3.70
$N1F$	-0.48	-1	0.074	0.0208	0.052	0.28	0.57	6.14	3.87
$N1M$	-0.48	-1	0.074	0.0208	0.056	0.28	0.55	6.07	3.80
$N2F$	-0.48	-2	0.074	0.0208	0.100	0.21	0.44	5.82	3.54
$N2M$	-0.48	-2	0.074	0.0208	0.110	0.20	0.40	5.63	3.49

Table 1: Roughness topographical statistics, where S_f is the total frontal projected area of the roughness. L_x^{corr} refers to the length scale where the roughness auto-correlation in streamwise direction drops under 0.2. Simulation results are shown on the last two columns on the right.

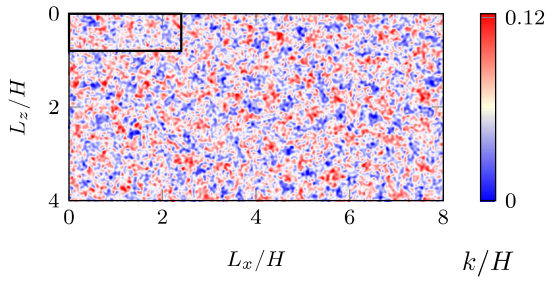

Figure 1: Full-span roughness sample $G2F$. The black rectangle represents the size of the minimal channel. Color bar shows the surface height.

profile. The definition of the zero plane displacement d in present work follows Jackson's method.

Effect of channel size

The velocity profile of exemplary cases $G2M$ and $G2F$ are compared in figure 2. The velocity offset profiles $U_s^+ - U_r^+$ are shown in the inset of figure 2 using same coloring style. With the same approach, temperature fields predicted by minimal channel and full span channel are compared in figure 3. As one can observe, excellent agreement of the profiles is achieved between minimal channels and full span channels below each critical height y_c. Due to the nature of minimal channels, an overestimation in the profiles in outer layer can be observed for both smooth and rough cases. However, the offset profiles for minimal channel and full span channel, as shown in the inset, collapse well and reach constant values in logarithmic layer. The roughness function ΔU^+ as well as $\Delta\Theta^+$ are obtained by measuring the mean offset of the profile in logarithmic layer, specifically over $y^+ = 160 - 250$.

Generalizing the observation to all considered cases, ΔU^+ along with $\Delta\Theta^+$ are summarized in the last two columns in table 1. To visualize the disagreement of minimal channel with full span channel, graphical comparison is illustrated in figure 4. It can be observed that minimal channels show excellent agreement with the conventional full span channels, the discrepancies of both ΔU^+ and $\Delta\Theta^+$ lie under 5%. Consistent predictions indicate the capability of the minimal channels in reproducing the hydrodynamics and thermal properties of the irregular pseudo-realistic roughness. The results also imply that both skin friction and heat transfer of a rough surface can be uniquely determined by the roughness PS and PDF.

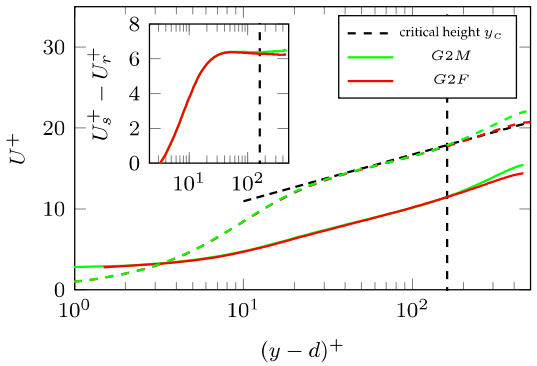

Figure 2: Mean velocity profile of roughness type $G2$, dashed line: velocity profile of smooth wall U_s^+, solid line: velocity profile of rough wall U_r^+. The inset shows the velocity retardation $U_s^+ - U_r^+$ as a function of wall normal distance $(y-d)^+$. Dash-dotted line represents Log-law.

Effect of roughness topography

Given the satisfactory performance of minimal channel simulations, in the following content the prediction results by minimal channels will be analysed. An overview of the roughness function ΔU^+ from minimal channel simulations is plotted in figure 5, where roughness function ΔU^+ is shown as a function of skewness Sk, grouped by the PS slope p. As investigated

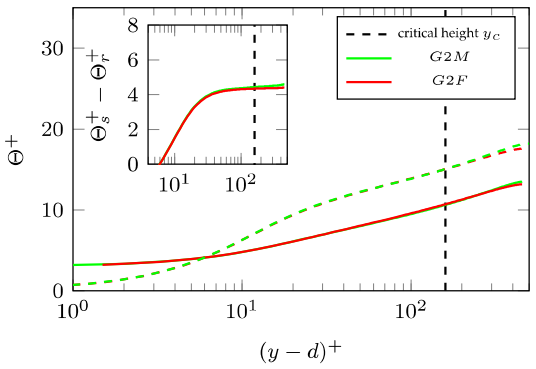

Figure 3: Mean temperature profile of roughness type $G2$, dashed line: temperature profile of smooth wall Θ_s^+, solid line: temperature profile of rough wall Θ_r^+. The inset shows the temperature retardation $\Theta_s^+ - \Theta_r^+$ as a function of wall normal distance $(y-d)^+$.

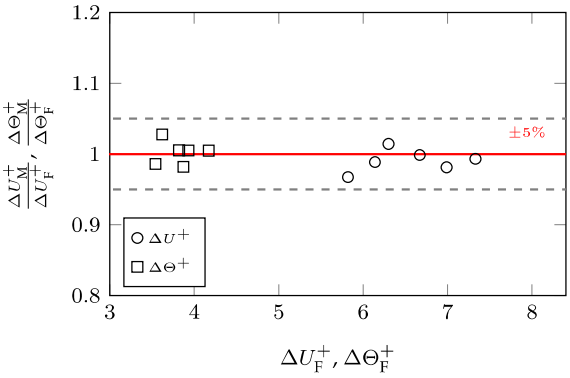

Figure 4: Comparison of the predictions by minimal channels with full span channels. ○: ΔU^+, □: $\Delta\Theta^+$. Gray dashed lines indicate the boundary of 5% error interval around $\Delta U_M^+/\Delta U_F^+ = \Delta\Theta_M^+/\Delta\Theta_F^+$=1

by Flack *et al.*(2020), positively skewed rough surfaces give higher skin friction than non-skewed or negatively skewed roughness. Negatively skewed surfaces show 'slip-velocity' effect (Jelly & Busse 2018), which translates into a weaker mean velocity retardation. The trend observed in the present results fully agrees with what suggested by the previous researchers.

On the other hand, the averaged offset of logarithmic temperature profile $\Delta\Theta^+$, analogous to ΔU^+, is shown by squares in figure 5. The evolution of $\Delta\Theta^+$ also shows monotonic increase with Sk. However, it is demonstrated that the variation of Sk affects $\Delta\Theta^+$ less significantly than ΔU^+. By adjusting the PS slope p the shift of $\Delta\Theta^+$ can be observed for all roughness topographies. To shed light into the correlation of spatial roughness distribution with ΔU^+ and $\Delta\Theta^+$, these values are plotted as a function of effective slope ES in figure 6. Approximately parallel increase of ΔU^+ and $\Delta\Theta^+$ with ES for all types of roughness are exhibited.

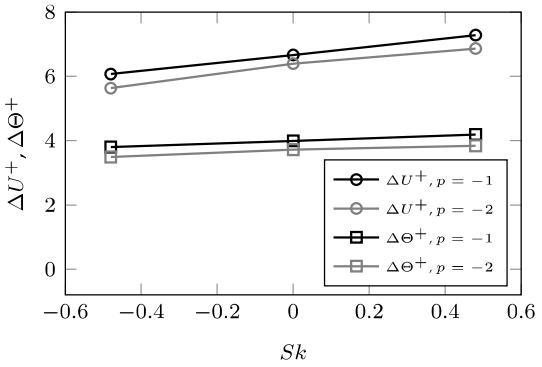

Figure 5: ΔU^+(circles) and $\Delta\Theta^+$(squares) predictions from minimal channels. Black: $p=-1$, gray: $p=-2$.

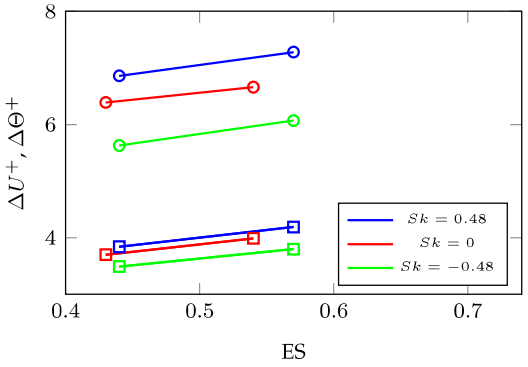

Figure 6: ΔU^+(circles) and $\Delta\Theta^+$(squares) predictions from minimal channels. Blue: $Sk=0.48$, red: $Sk=0$, green: $Sk=-0.48$.

4 Conclusions

DNS is carried out for fully developed turbulent channel with artificial irregular roughness at $Re_\tau \approx 500$. A passive scalar is added to simulate the temperature field. The rough surfaces are generated based on the mathematical roughness generation method proposed by Ràfols & Almqvist(2019). Three types of roughness PDF, namely $Sk=-0.48$, 0, 0.48 are combined with 2 types of power-law roughness PS whose slope $p=-1$& -2. It is demonstrated that the minimal channel is capable of reproducing the hydrodynamic and thermal properties of the artificial irregular roughness with significant reduction in computational effort. In the present work, the roughness function ΔU^+ and the offset of temperature profile in logarithmic layer $\Delta\Theta^+$ are compared among considered types of roughness topographies with systematically adjusted PDF and PS. Simultaneous increase of ΔU^+ and $\Delta\Theta^+$ for

different types of roughness can be observed with increasing ES. A monotonic increase of ΔU^+ as a function of Sk is observed, similar trend can be observed for $\Delta\Theta^+$. However, the influence of Sk on the temperature profile shows less significance than the influence on the velocity profile. The different behavior of $\Delta\Theta^+$ calls for a detailed study on the temperature field of turbulent flow over rough surfaces.

Acknowledgments

Support by DFG project number CRC TRR 150 as well as the Friedrich-and-Elisabeth-Boysen Foundation (BOY-151) is greatly acknowledged. This work was performed on the supercomputer ForHLR and the storage facility LSDF funded by the Ministry of Science, Research and the Arts Baden-Württemberg and by the Federal Ministry of Education and Research.

References

Jiménez, J. (2004), Turbulent flows over rough walls, *Ann. Rev. Fluid Mech.* Vol. 36, pp. 173-196.

Hama, F.R. (1954), Boundary-layer characteristics for rough and smooth surfaces, *Soc. Nav. Archit. Mar. Eng.* Vol. 64, pp.333.

Flack, K. A. and Schultz, M. P. (2010), Review of Hydraulic Roughness Scales in the Fully Rough Regime, *J. Fluids Engineering*, Vol. 132.

Napoli, E., Armenio, V. and De Marchis, M (2008). The effect of the slope of irregularly distributed roughness elements on turbulent wall-bounded flows, *J. Fluid Mech.*, Vol. 613. pp. 385-394.

Sigal, A., Danberg, J. E. (2008), New correlation of roughness density effect on the turbulent boudnary layer, *AIAA Journal*, Vol. 28, pp. 554-556.

Forooghi, P., Flory, M., Bertsche, D., Wetzel, T. and Frohnapfel, B. (2017a). Heat transfer enhancement on the liquid side of an industrially designed flat-tube heat exchanger with passive insertes-numerical investigation. *Appl. Therm. Eng.*, Vol. 123, pp. 573-583.

Dipprey, D. F. and Sabersky, R. H. (1963), Heat and momentum transfer in smooth and rough tubes at various prandtl numbers. *Int. J. Heat Mass Transfer.* Vol.6, pp. 329-353.

Bons, J.P. (2005) A critical assessment of Reynolds analogy for turbine flows. *ASME J. Heat Transf.*, Vol. 127(5), pp. 472-485.

MacDonald, M., Hutchins, N., Chung, D. (2019), Roughness effects in turbulent forced convection, *J. Fluid Mech.*, Vol. 861, pp. 138-162.

Flack, K. A. (2018), Moving beyond Moody, *J. Fluid Mech.*, Vol. 842, pp. 1-4.

Chung, D., Chan, L., MacDonald, L., Hutchins, N. and Ooi, A. (2015), A fast direct numerical simulation method for characterising hydraulic roughness, *J. Fluid Mech.*, Vol. 773, pp. 418-431.

MacDonald, M., Chung, D. Hutchins, N., Chan, L., Ooi, A. and García-Mayoral, A. (2016), The minimal channel: a fast and direct method for characterising roughness, *Journal of Physics: Conference Series*, Vol. 708,

Pérez-Ràfols, F. and Almqvist, A. (2019), Generating randomly rough surfaces with given height probability distribution and power spectrum, *Tribology International*, Vol. 131, pp. 591-604.

Goldstein, D., Handler, R. and Sirovich, L., Modeling a no-slip flow boundary with an external force field, *Journal of Computational Physics*, Vol. 105, pp. 354-366.

Kasagi, N., Tomita, Y., Kuroda, A. (1992), Direct numerical simulation of of passive scalar field in a turbulent channel flow, *Journal of Heat Transfer*, Vol. 114(3), pp. 598-606.

Barros, J. M., Schultz, M. P. and Flack, K. A. (2018), Measurements of skin-friction of systematically generated surfaces roughness,*Intl. J. Heat and Fluid Flow*, Vol. 72, pp. 1-7.

Nikora, V. I., Stoesser, T., Cameron, S. M., Stewart, M., Papadopoulos, K., Ouro, P., McSherry, R.,Zampiron, A., Marusic, I., Falconer, R. A. and et al (2019), Friction factor decomposition for rough-wall flows: theoretical background and application to open-channel flows, *J. Fluid Mech.*, Vol. 872, pp. 626-664.

Jackson, P.S. 1981 On the displacement height in the logarithmic velocity profile. *J. Fluid Mech.* vol.111, pp.15-25.

Flack, K.A., Schultz. M.P. & Barros, J.M. 2020 Skin friction measurements systematically-varied roughness: Probing the role of roughness amplitude and skewness. *Flow, Turbulence and Combustion*, Vol. 104, pp.317-329.

Jelly, T.O. & Busse, A. 2018 Reynolds and dispersive shear stress contributions above highly skewed roughness *J. Fluid Mech.* vol. 852, pp. 710-724.